RSC Advances

PAPER

View Article Online
View Journal | View Issue

Cite this: *RSC Adv.*, 2021, **11**, 17727

Dendronized oligoethylene glycols with phosphonate *tweezers* for cell-repellent coating of oxide surfaces: coarse-scale and nanoscopic interfacial forces†

Julian Czajor,‡[a] Wasim Abuillan,‡[a] Dinh Vu Nguyen,[b] Christopher Heidebrecht,[a] Evan A. Mondarte,[c] Oleg V. Konovalov,[d] Tomohiro Hayashi,[ce] Delphine Felder-Flesch,[bf] Stefan Kaufmann[a] and Motomu Tanaka*[ag]

Received 1st April 2021
Accepted 10th May 2021

DOI: 10.1039/d1ra02571f

rsc.li/rsc-advances

Dendronized oligoethylene glycols (dendron OEGs) with two phosphonate groups (phosphonate *tweezers*) have been drawing significant attention as a new class of coating materials for superparamagnetic iron oxide surfaces. However, despite dendron OEGs showing outstanding stability in physiological fluids in previous studies, little is understood about their structure and mechanical properties. Herein we report the surface and internal structures and mechanical properties of dendron OEGs, and quantitatively determine their ability to avoid non-specific adhesion of blood platelets. To gain insight into the interfacial force interactions, we measured the coarse-scale surface force acting on cell-sized particles and mapped the nanoscopic pinning centers by fast force mapping.

Introduction

Owing to their excellent magnetic properties and high transverse relaxation, over the past several decades superparamagnetic iron oxide nanoparticles have been drawing increasing attention for a variety of medical applications, such as contrast enhancement in MRI[1–3] and hyperthermia cancer theranostics.[4,5] A key prerequisite for their medical application is the chemical functionalization of nanoparticles to achieve; (i) high stability in physiological fluids, (ii) control of the particle size below 100 nm, without aggregation, and (iii) the preservation of high saturation magnetization. In the absence of surface coating materials, iron oxide nanoparticles tend to form μm-sized aggregates. In addition, it is clear that iron oxide nanoparticles for medical applications should not non-specifically adhere to vascular endothelial cells or blood cells, particularly platelets. To date, several polymers have been developed for coating the surface of oxide nanoparticles, including polyethylene glycol (PEG),[6] dextran,[7] and polyvinylpyrrolidone, amongst others.[8] However, despite significant progress, a persisting limitation of polymer-based coatings is that high molecular weight polymers tend to form thick organic "shells" that generally increase the hydrodynamic diameter of particles and cause problems following administration.

To increase the grafting density and enable the flexible adjustment of structures and functions, Felder-Flesch and coworkers proposed the grafting of dendritic oligoethylene glycols *via* phosphonate chemistry.[9–11] In contrast to widely-used linear polymer brushes, dendritic molecules allow for the discrete control of entities with monodisperse size and physical properties by changing their generation.[12] Phosphonates were chosen for the surface coupling because they realize a much higher grafting rate[13] and stronger binding than the carboxylate anchors more commonly used for the surface coating of oxide nanoparticles.[14,15] The replacement of carboxylates with phosphonates also offers an advantage in terms of the magnetic properties. In-field Mössbauer spectroscopy and SQUID measurements have suggested that the coating of oxide with carboxylates leads to spin canting in the oxide layer, resulting in a decrease in the net magnetization. In contrast, coating with phosphonate did not screen the magnetic properties.[15] The coating of iron oxide nanoparticles with thin layers of dendronized oligoethylene glycol *via* phosphonate chemistry therefore realized versatile, robust, and high relaxation MRI contrast agents.[10] To date, dendronized

[a]*Physical Chemistry of Biosystems, Institute of Physical Chemistry, Heidelberg University, 69120 Heidelberg, Germany. E-mail: tanaka@uni-heidelberg.de*
[b]*Institut de Physique et Chimie des Matériaux de Strasbourg (IPCMS), University of Strasbourg, 23 rue du Loess, 67034 Strasbourg, France*
[c]*Department of Materials Science and Engineering, School of Materials and Chemical Technology, Tokyo Institute of Technology, 226-8502, Kanagawa, Japan*
[d]*European Synchrotron Radiation Facility, CS 40220, 38043, Grenoble, France*
[e]*JST-PRESTO, 4-1-8 Hon-cho, Kawaguchi, Saitama, 332-0012, Japan*
[f]*SUPERBRANCHE SAS, IPCMS Bâtiment 69, 23 rue du loess BP 43, 67034 Strasbourg Cedex 2, France*
[g]*Center for Integrative Medicine and Physics, Institute for Advanced Study, Kyoto University, Kyoto 606-8501, Japan*

† Electronic supplementary information (ESI) available. See DOI: 10.1039/d1ra02571f

‡ Equal contributors.

oligoethylene glycol layers on iron oxide nanoparticles have been characterized using thermal analysis (TGA and DTA), FTIR, and XPS. Although the outstanding stability of nanometer-thick dendron layers under physiological conditions—such as in blood—indicates their potential for use as ultrathin cell-repellent coating materials, little is understood of how their physical characteristics modulate interactions with cells.

In this study, we investigate the structure and mechanical properties of dendronized oligoethylene glycol layers grafted on planar silica surfaces by combining various surface sensitive techniques. We studied two dendronized oligoethylene glycols, denoted dendron OEG4 and dendron OEG8 (Fig. 1a).[11] These molecules contain two phosphonate groups, known as "phosphonate tweezers", that realize stronger surface coupling than a single phosphonate group. First, we optimized the preparation conditions by slightly modifying a previously reported protocol.[16] After optimizing the functionalization protocols, we determined the surface topography and internal structures of the dendron OEG films in air and in buffer using AFM and high energy specular X-ray reflectivity, respectively. The mechanical properties of the dendron OEG films were further characterized by nanoindentation. As surface coating with both dendronized OEGs distinctly reduced the non-specific adhesion of human platelets, we tried to determine the physical mechanism of cell repellency. First, we measured the Young's modulus of the dendron OEG monolayers using AFM nanoindentation. To understand the interfacial forces exerted on cells near the dendron-coated surfaces, we measured the coarse-scale surface forces using a cantilever connected to a cell-sized SiO_2 particle. In addition, we carried out fast force mapping to spatially resolve the nanoscopic pinning centers that are much smaller than a single cell.

Results and discussion

Optimization of functionalization, and surface topography

We initially functionalized the surface of Si wafers by incubating the substrates with an aqueous solution of dendrons (1 mg mL^{-1}) for 30 min, according to a previously reported protocol.[11] However, the resulting film exhibited numerous defects (ESI Fig. S1†), suggesting that the film deposition protocol required improvement. We therefore followed a protocol reported by Hanson *et al.*, *tethering by aggregation and growth*, which was developed for hydrophobic phosphonates.[16]

To optimize the protocol for our dendrons, we systematically varied the reaction time, temperature, and heating time. The quality of the dendron coating was assessed by water contact angle (θ) and ellipsometry measurements. After optimizing each parameter (for the full protocol see the Experimental section), we were able to reproducibly prepare films with a water contact angle of $\theta = 30$–40° and ellipsometric thickness of $d = 9$–12 Å, which suggests the deposition of monolayers that present oligoethylene glycol chains.

The surface topographic profiles of Si wafers coated with dendrons OEG4 and OEG8 were characterized using tapping mode AFM. Fig. 1b and c show the representative topographic profiles of a dendron OEG4 film measured in air and in buffer, respectively. The rms roughness value calculated within a 5×5 μm^2 area in air ($\sigma \approx 2$ Å) confirmed the uniform grafting of dendron molecules. In buffer, the rms roughness increased slightly to $\sigma = 6$ Å, which is attributed to hydration of the layer. The corresponding data for dendron OEG8 measured in air and buffer are presented in Fig. 1d and e, respectively. It should be noted that the optimized functionalization protocol resulted in much higher film quality than was achieved by simple immersion of the substrate in an aqueous solution. The detailed AFM data are presented in ESI Table S1.†

Internal structure of the dendron layers

The internal structures of dendron OEG monolayers perpendicular to the surface were investigated using high energy specular X-ray reflectivity. The use of high energy X-rays (22 keV) guarantees the transmittance of the beam through bulk water.[17,18] Fig. 2a shows the reflectivity curves of the dendron OEG4 (red) and OEG8 (blue) monolayers measured in air. The reflectivity curves, plotted as Rq_z^4, exhibited features indicating the formation of layered structures with distinct contrast in scattering length density (SLD). The best fit results (solid lines) obtained with a slab model yielded a layer thickness of dendron

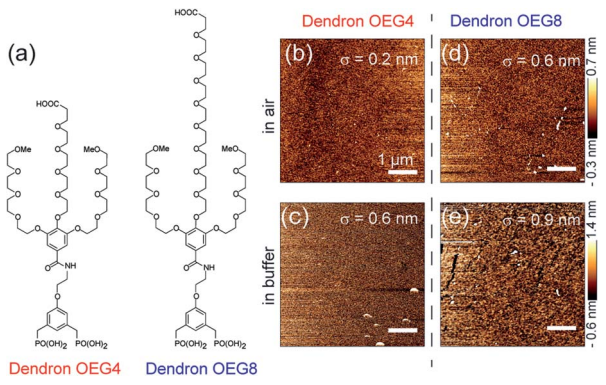

Fig. 1 (a) Chemical structures of dendron OEG4 and dendron OEG8. Tapping mode AFM images of dendron OEG4 (b) in air and (c) in buffer. The corresponding data for dendron OEG8 are shown in panels (d) and (e), respectively. Roughness rms values calculated within 5×5 μm^2 confirmed the formation of uniform films. Scale bars: 1 μm.

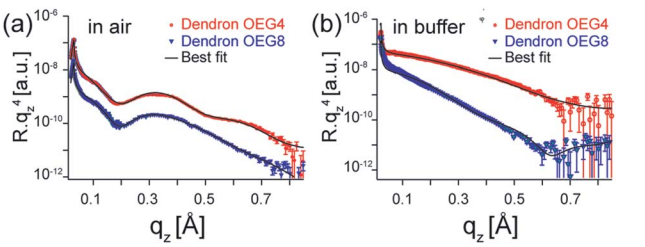

Fig. 2 High energy specular X-ray reflectivity (symbols) and best-fit results (lines) of dendron OEG4 (red) and dendron OEG8 (blue) measured (a) in air and (b) in buffer. The data collected in air are fitted with slab models, while those measured in buffer with diffusive interface models (eqn (1)). The structural parameters corresponding to the fits are presented in Tables 1 and 2, confirming the formation of monolayers.

Table 1 Thickness d, SLD and roughness σ of OEG films in air as determined by XRR analysis using a slab model

	d [Å]	SLD [10^{-6} Å^{-2}]	σ [Å]
Dendron OEG4	14.6	8.17	6.5
Dendron OEG8	14.9	11.6	3.1

OEG4 of $d_{OEG4} = 14.6$ Å. Despite having additional ethylene glycol units, the thickness of the dendron OEG8 layer was almost the same, $d_{OEG8} = 14.9$ Å. This observation is attributed to the collapse of the oligoethylene glycol chains under the osmotic pressure in ambient atmosphere. The SLD of dendron OEG8 was approximately 1.4 times greater than that of dendron OEG4 (Table 1), indicating the compaction of the OEG8 chains.

In contrast, as presented in Fig. 2b, the reflectivity curves measured in buffer exhibited no marked features for either dendron. In buffer, the transition of SLD from the dendron layer to bulk water becomes diffusive, which makes the use of the conventional slab model with Gaussian roughness invalid. In this study, the SLD profile was modeled by a hyperbolic tangent function,

$$\rho(z) = \rho_w + \frac{1}{2}(\rho_s - \rho_w)[1 + \tanh((z - z_0)/\xi)] \quad (1)$$

where ρ_w is the SLD of water, ρ_s is the SLD of the substrate, z_0 is the position of the layer center, and ξ is the decay parameter. Previous studies have suggested that the refractive index near the liquid/vapor interface can be represented by a hyperbolic tangent function.[19,20] In addition, Binder showed that the volume fraction of polymers near the interface should follow the hyperbolic tangent function.[21] We split the analytical SLD profile into a set of 1 Å-thick slabs, and the reflectivity curve was computed as a function of q_z using the Abelès formalism.[22,23] The best fit results are shown by solid lines in Fig. 2b, and the thickness and the decay parameter ξ are summarized in Table 2. Note that the film thickness was determined from the full width at half maximum (FWHM) of the Gaussian function used to fit the first derivative of the SLD profile (ESI Fig. S2†). Both the thickness and decay parameters of dendron OEG8 were greater than those of dendron OEG4, which seems reasonable given the presence of additional ethylene glycol units (Fig. 1a).

Mechanical characterization of dendron OEG monolayers

We evaluated the mechanical properties of the dendron monolayers using AFM nanoindentation with a cantilever coupled to a 10 μm SiO_2 particle.[24] It is well established that AFM indentation data for a thin film on a stiff substrate cannot be treated with a conventional Hertz model with a spherical indenter[24] as the film deformation is limited under a high load.[25,26] In this study, we assumed a transition function that linearly connects the influence of two elastic layers, the monolayer and the substrate,[27,28]

$$\frac{1}{E} = \frac{(1 - e^{\alpha\delta/d})}{E_M} + \frac{e^{\alpha\delta/d}}{E_S} \quad (2)$$

where E is the composite Young's modulus, and E_M and E_S are the Young's moduli of the monolayer and substrate, respectively. δ is the indentation depth, and d is the thickness. α is an empirically determined parameter that characterizes the sharpness of the transition. As presented in Fig. 3a, a decrease in α is accompanied by the broadening of the transition.[28] Fig. 3b shows the indentation–force relationships for dendrons OEG4 and OEG8 measured in buffer. The solid lines show the best fit results obtained by the systematic variation of E_M and α, while keeping the substrate elasticity constant (172 GPa). Fig. 3c shows the relationships between indentation depth and Young's modulus for the two monolayers, and clearly indicates that the Young's modulus is not constant once the indentation depth exceeds a certain level. We obtained Young's moduli of $E_{OEG4} = 1.3$ GPa, and $E_{OEG8} = 1.8$ GPa from the regions showing constant elasticity levels.

Platelet adhesion on dendron-coated surfaces

Fig. 4a–d show representative glutaraldehyde-induced fluorescence technique (GIFT)[29,30] images of (a) bare glass, (b) glass coated with hydrophobic octadecyltrimethoxysilane (ODTMS), (c) glass coated with dendron OEG4 and (d) glass coated with dendron OEG8, after incubation with platelets. The global appearance of the images suggests less platelet adhesion on the dendron-coated surfaces than on either hydrophilic glass or hydrophobic silane. Moreover, the images at higher magnification (bottom row) suggest that the spreading and hence the activation of platelets is also less pronounced on dendron-coated surfaces. Fig. 4e shows the number of platelets adhered to a 1 mm^2 surface, calculated from $N > 120$ images for each surface. On hydrophilic glass and hydrophobic ODTMS surfaces, we found median values of 5000–6000 cells per mm^2. In comparison, the corresponding values on dendron-coated surfaces were significantly lower; 2000–3000 cells per mm^2 ($p <$

Table 2 Thickness and dimensionless decay parameter of OEG films in buffer as determined by XRR analysis using a diffuse interface model

	d [Å]	ξ
Dendron OEG4	21.1	11.6
Dendron OEG8	29.1	16.9

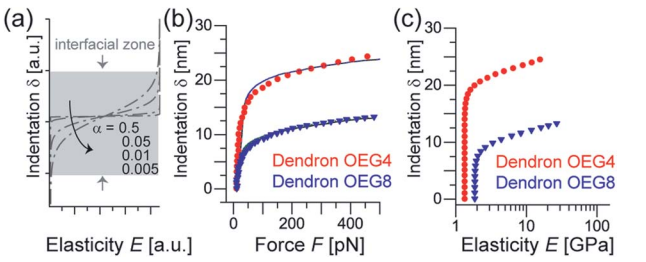

Fig. 3 (a) Elasticity profile of an interfacial zone between two phases possessing different levels of elasticity (eqn (2)). Decrease in transition parameter α results in slower transition. (b) Indentation–force relationships for dendron OEG4 (red symbols) and dendron OEG8 (blue symbols) with the best fit results (solid lines). (c) Dependence of Young's modulus of two dendrons as a function of indentation depth. The apparent film elasticity values were determined from the regions where Young's modulus is independent from indentation depth. Interface model.

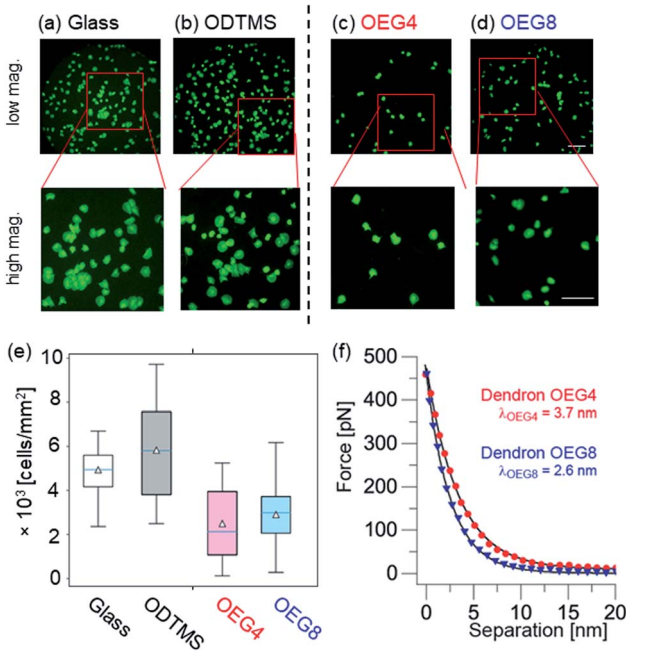

Fig. 4 Glutaraldehyde-induced fluorescence technique (GIFT) images of platelets adhered on (a) bare glass and glass coated with (b) hydrophobic silane (octadecyltrimethoxysilane, ODTMS), (c) dendron OEG4 and (d) dendron OEG8. Images with higher magnifications are shown in lower panels, suggesting that the adhesion and spreading of platelets are suppressed on dendron-coated surfaces. Scale bars: 25 μm. (e) Surface density of adhered platelets (N > 100 images per condition), indicating that both dendrons could suppress the non-specific adhesion of platelets. (f) Force–separation relationships of dendrons OEG4 (red) and dendron OEG8 (blue) measured by AFM cantilever coupled to silica particle ($\Phi \approx 10$ μm).

0.001). This clearly indicates that the coating of substrates with nanometer-thick dendron monolayers effectively suppresses non-specific adhesion of platelet cells. The data indicated that there were more platelets on dendron OEG8 surfaces than on OEG4, however the difference was less significant ($p \approx 0.02$).

Rodrigues *et al.* functionalized Au surfaces with thiol monolayers that contained various fractions of molecules with CH_3- and OH-terminal groups.[30] They observed the highest and lowest numbers of adherent platelets on pure CH_3- and OH-terminated monolayers, respectively. By systematically varying the mixing ratio of the hydrophobic (CH_3-terminated) and hydrophilic (OH-terminated) thiols, they concluded that platelet adhesion is highly sensitive to the surface free energy. However, as shown in Fig. 4, the dendron-coated surfaces showed distinctly lower non-specific adhesion than bare glass substrates and substrates coated with hydrophobic ODTMS, suggesting that the cell repellency does not correlate with the surface free energy. Using thiol monolayers terminated with single oligoethylene glycol chains, a more recent study demonstrated that the surface free energy correlates with non-specific adsorption of proteins but not with non-specific cell adhesion.[31]

To unravel the origin of platelet repellency from the viewpoint of interfacial forces, we analyzed the force-separation curves obtained using an AFM cantilever coupled to a 10 μm SiO_2 bead.[24] Unlike for the "indentation" analysis presented in Fig. 3, we focused on the region before the probe made the first contact with the surface. Fig. 4f shows force-separation curves for dendron OEG4 and dendron OEG8. It is notable that the detected forces always remain positive, which indicates that the interfacial interaction is predominantly repulsive. The absence of any attractive, negative force was confirmed over the whole surface of each sample. In Fig. 4f, we defined the separation $s = 0$ as the position at which the interfacial force reached 450 pN because the force curves converge beyond this threshold. The onset of the force increase appears at a distance that is greater than the film thickness obtained by X-ray reflectivity (Table 2), suggesting the presence of a repulsive zone in close proximity to the surface. To estimate how far such repulsion could reach, we fitted the force curves as exponential decay functions and calculated the characteristic decay length λ. Interestingly, the decay length λ of dendron OEG4, $\lambda_{OEG4} = 3.7$ nm, was greater than that of OEG8, $\lambda_{OEG8} = 2.6$ nm, suggesting that the repulsive force field of the shorter dendron OEG4 extended further than that of the longer dendron OEG8.

The presence of a repulsive layer near the bio-inert surfaces was also reported for Au substrates coated with alkanethiols terminated with linear oligoethylene glycols.[31] The origin of the repulsive zone was attributed to a layer of "structured interfacial water". Despite the qualitative agreement with their finding, the repulsive zone we observed cannot be explained by a layer of structured water. It is widely accepted that linear oligoethylene glycols connected to alkanethiols adopt an ordered conformation, particularly with the aid of attractive interactions between the hydrocarbon chains.[32] Conversely, as our dendron molecules are grafted to the oxide surface *via* bulkier phosphonate tweezers (Fig. 1a), the grafting density of molecules is much lower than for linear ethylene glycols connected to alkanethiols. As the branched ethylene glycol chains are not able to adopt an ordered conformation owing to steric constraints, the dendron surface cannot support the formation of structured interfacial water. A possible candidate for creating the repulsive zone is the entropic force generated by thermally activated conformational dynamics of the OEG chains. In fact, the X-ray reflectivity data suggest that the interface between the dendron monolayer and bulk water is diffusive (Fig. 2b, Table 2).

Nanoscopic force mapping

It is notable that platelets still adhere to the dendron-coated surfaces (Fig. 4c and d) despite the repulsive zone near the surface. This suggests the presence of local potential minima (pinning centers) that cause non-specific platelet adhesion. Thus, we extended our understanding of the modulation of coarse-scale interfacial interactions by dendrons to investigate if such local pinning centers exist. We performed fast force mapping experiments at a pixel rate of 200 Hz.[33] Fig. 5a shows typical force curves collected from one pixel during the wave-like motion of the cantilever. The broken line is the curve collected during the approach, while the solid line shows the retraction. As indicated in the figure, we defined the difference between the baseline and the force minimum in retraction as the adhesion force. Fig. 5b shows the histograms of adhesion

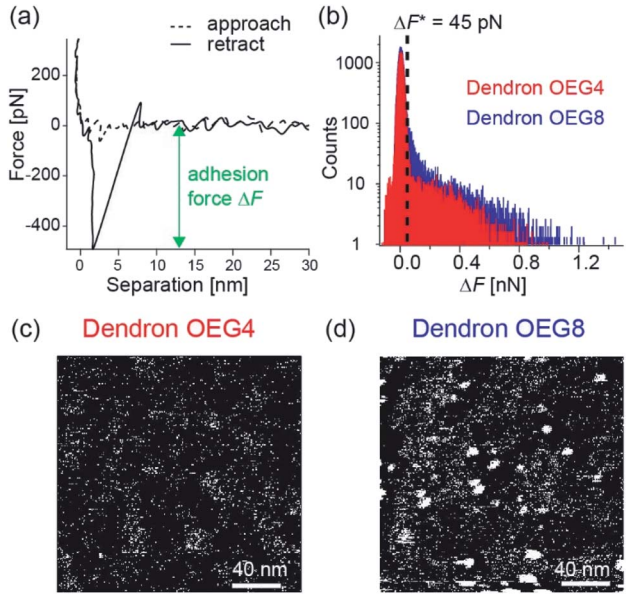

Fig. 5 (a) A representative nanoscopic fast force curves during the approach (broken line) and retraction (solid line) collected at a pixel rate of 200 Hz. Difference between the baseline and the force minimum in retraction is defined as adhesion force ΔF. (b) Histograms of ΔF for dendron OEG4 (red) and dendron OEG8 (blue). The threshold level ($\Delta F^* = 45$ pN) is indicated by a broken line. Binarized fast force maps for (c) dendron OEG4 and (d) dendron OEG8. White regions coincide with pinning centers, corresponding to $\Delta F > 45$ pN. Dendron OEG4 surface shows only pixel noises, while approx. 10 nm-large pinning centers can be identified on dendron OEG8.

force for dendron OEG4 (red) and dendron OEG8 (blue) and the threshold values of $\Delta F^* = 45$ pN indicated by a broken line. Fig. 5c and d are binarized force maps for dendron OEG4 and dendron OEG8, respectively. Here, the pixels with $\Delta F > 45$ pN are labeled white, while the rest are black. The surface coated with dendron OEG4 exhibited pixel noise (Fig. 5c), but distinct, approximately 10 nm spots can be identified on the surface coated with dendron OEG8 (Fig. 5d).

It is plausible that 10 nm pinning centers found in the dendron OEG8 monolayer coincide with the regions of lower grafting density but not the defects. In fact, the rms roughness values for dendron OEG4 and dendron OEG8 obtained by tapping mode AFM are comparable (Fig. 1d and e). Moreover, X-ray reflectivity data in buffer (Fig. 2b) indicated no sign of local defects because the beam footprint was much larger than the pinning centers. However, the Young's modulus of the dendron OEG8 monolayer was higher than that of dendron OEG4 (Fig. 3), which appears to reflect the lower grafting density of dendron OEG8. Although the size of the pinning centers detected by nanoscopic fast force mapping was much smaller than silica particles and platelet cells, this appears to explain the higher platelet density observed on the dendron OEG8 surfaces (Fig. 4e). The observation that platelets can detect 10 nm pinning centers while silica particles cannot, is attributed to the difference in the deformability. Lipid membranes surrounding cells possess low bending rigidity $\kappa \sim 10 k_B T$ (ref. 34) so that cells can adapt their shape to the surrounding environment. In fact, as shown in Fig. 4a–d, platelets adhered to the surface were flattened, and some even exhibited spreading due to activation. Conversely, SiO_2 particles are not sensitive to such nanoscopic surface heterogeneities because the deformability of the particle is negligibly small.

Water molecules confined near surfaces have been drawing increasing attention because of their physical characteristics distinct from those in the bulk.[35–37] Using frequency modulation AFM, Jarvis and co-workers identified layered water near the surface of crystalline-like, carboxyl-terminated thiol monolayers as oscillatory force signals separated at a distance of $\approx$0.25 nm.[38] Inada *et al.* took a similar approach on highly ordered monolayers of oligoethylene glycol chains connected to alkanethiols.[32] Although they successfully observed highly ordered oligoethylene glycol chains, layered water molecules near the surface were not detected. More recently, Araki *et al.* used the same technique, and reported the presence of structured water near the surface of monolayers displaying a mosaic of cationic and anionic head groups, but not near CH_3- or COOH-terminated surfaces.[39] In this study, our force-separation curves exhibited no sign of oscillatory features originating from a structured water layer, suggesting that water molecules near the surfaces were not structured owing to the amorphous nature caused by the bulkier phosphonate anchoring groups, the lack of cohesive hydrocarbon chains, and branches.

Experimental

Materials and sample preparation

Materials. The dendrimers were synthesized as previously described.[11] One side-polished Si [100] with thermal and native oxides (Si Mat, Landsberg am Lech, Germany) were used as substrates. Unless otherwise stated, all chemicals were purchased from Sigma-Aldrich (Munich, Germany) and used without further purification. Double deionized water (MilliQ, Molsheim, France) with a specific resistance of $\rho > 18$ MΩ cm was used throughout this study.

Surface functionalization. Si substrates were cleaned by RCA cleaning and immersed in dendrimers dispersed in anhydrous THF (1 mM) for 1 h under reflux (80 °C). The samples were then transferred to a vacuum oven and heated at 145 °C for 10 min to establish the covalent bonding. Then, the unbound molecules were removed by sonication in THF and EtOH (10 min each). After rinsing with water, the samples were kept in a vacuum chamber.

Assessment of film quality. To optimize the preparation protocols, the film thicknesses were measured using a Multiskop ellipsometer (Optrel, Kleinmachnow, Germany) at $\lambda = 632.8$ nm and $\alpha_i = 70°$. The refractive indices of Si, SiO_2, and dendrimer were $n_{Si} = 3.87–0.016i$, $n_{SiO_2} = 1.457–0i$, and $n_{dendrimer} = 1.466$. The water contact angle was also measured using a Multiskop equipped with a back light and CCD camera. The contact angle of a water droplet (volume: 2 μL) was calculated using the ImageJ plug-in.

Experimental methods

Tapping mode atomic force microscopy (AFM). Topographic profiles of the dendrimer-coated surfaces were characterized

using a NanoWizard 3 AFM (JPK, Instruments AG, Berlin, Germany) in tapping mode at 293 K. The measurements in air were performed using NCHV-A cantilevers with a spring constant of $k = 42$ N m^{-1} and a tip radius of $r < 8$ nm, while the measurements in buffer were carried out with SNL-10 cantilevers with a spring constant of $k = 0.35$ N m^{-1} and a tip radius of $r < 12$ nm (Bruker, Karlsruhe, Germany).

High energy specular X-ray reflectivity. X-ray reflectivity measurements were carried out at the ID10 beamline of the European Synchrotron Radiation Facility (ESRF, Grenoble) at 293 K. The samples were irradiated with a monochromatic synchrotron beam with an energy of 22 keV ($\lambda = 0.56$ Å),[17,18] and the signal was recorded with a linear position sensitive detector (Mythen 1K, Dectris, Switzerland). The reflectivity data measured in air were analyzed using a genetic minimization algorithm implemented in the MOTOFIT/Igor package (Wavemetrics, OR, USA). As the data measured in buffer could not be analyzed with the standard slab model owing to the diffusive nature of the interface, we modeled the SLD profiles near the interface using a hyperbolic tangent function.[21] The analytical SLD profile was split into slabs with 1 Å thickness. Since this is close to the instrument resolution, it was not necessary to include slab roughness in these calculations.[40] The reflectivity curve was computed as a function of q_z using the Abelès formalism,[22,23] using a self-written fitting algorithm in Igor (Wavemetrics, OR, USA).

AFM nanoindentation. Nanoindentation experiments were performed at 293 K on a NanoWizard 3 AFM (JPK, Instruments AG, Berlin, Germany) using a cantilever coupled to a 10 μm SiO_2 particle (Thermo Scientific Particle Technology, CA, USA). To avoid artifacts from limited film deformation, we represented the composite compliance of the dendron layer and the substrate as a linear combination weighted with a transition function (eqn (2)).[27,28]

Platelet adhesion experiments. Prior to the experiments, platelets were pelleted twice by centrifugation for 20 min (800 × *g*) in Tyrode's solution (134 mM NaCl, 12 mM $NaHCO_3$, 2.9 mM Na_2HPO_4, 1 mM $MgCl_2$, 10 mM HEPES, pH 7.4) containing 5 mM glucose, 3 mg mL^{-1} bovine serum albumin (BSA), and 0.2 U mL^{-1} apyrase to prevent platelet activation. Platelet concentrations were determined using a Thoma counting chamber (Brand GmbH, Wertheim, Germany) and adjusted to 2.5×10^7 cells per mL. Before exposure to the substrates, we briefly checked the sample using bright field microscopy and confirmed that the platelets were not activated during the preparation. The surfaces were first incubated with a 2 mL sample of 1% human plasma at 293 K for 30 min and then washed three times with buffer. In the next step, a 1 mL sample of platelet suspension was allowed to react with the surface at 273 K on a shaker (70 rpm). After incubation for 30 min, the substrates were washed three times with buffer. For the glutaraldehyde-induced fluorescence technique (GIFT) imaging,[29,30] the cells were fixed with 2 mL of freshly prepared 2% glutaraldehyde solution for 30 min. After fixation, the samples were washed three times with buffer and once with water. The phase contrast (ESI Fig. S3†) and GIFT images were collected using an Axioobserver (Zeiss, Oberkochen, Germany) equipped with a 63× oil immersion objective. To guarantee the statistical reliability, $N > 120$ images were collected for each sample. The adhesion behavior of the platelets was determined from the number of adherent platelets in a 1 mm^2 area.

Surface force measurements. Force-separation curves ($N >$ 100 curves for each sample) were recorded at 293 K using an MFP-3D Bio AFM (Oxford Instruments, MA, USA). A 10 μm SiO_2 particle (Thermo Scientific Particle Technology, CA, USA) was coupled to a V-shaped tipless cantilever ($k = 0.06$ N m^{-1}, Veeco, NY, USA). The approach speed of the colloidal microparticle was set at a constant 400 nm s^{-1}, and the triggering force was set at 500 pN. The deflection sensitivity was assessed from the force–distance curve in the linear compliance region (<1 nN), and the point of zero separation was set as the position where the linearity in the constant compliance region started to deviate more than 10%.

Nanoscopic fast force mapping. Local surface forces and height profiles were mapped at a pixel rate of 200 Hz using an MFP-3D Infinity AFM (Oxford Instruments, MA, USA). Here we used cantilevers (BioLever mini, Olympus, Tokyo, Japan) with a Si apex and $k = 0.09$ N m^{-1}, calibrated using a thermal noise method.[41] This mode of measurement enabled the simultaneous acquisition of topographic images and force profiles pixel-to-pixel using a continuous wave-like motion of the cantilever.

Conclusions

The grafting of dendronized oligoethylene glycols (dendron OEGs) with phosphonate tweezers is a promising approach for assembling highly stable, ultrathin coating materials that suppress the non-specific adhesion of cells. In this study, we carefully optimized the functionalization protocols and systematically investigated the surface and internal film structures by combining tapping mode AFM and high energy specular X-ray reflectivity. The diffusive scattering length density profiles of the nanometer-thick dendron OEG monolayers were modeled with a hyperbolic tangent function instead of commonly used slab models. The Young's modulus of the monolayers was assessed by AFM nanoindentation with a cantilever coupled to a 10 μm SiO_2 particle. To account for the limited deformation of ultrathin films under high loads, we used a transition function that linearly connects the elastic properties of monolayers and solid substrates. The statistical analysis of images collected by glutaraldehyde induced fluorescence technique (GIFT) demonstrated that both dendrons, OEG4 and OEG8, significantly suppressed the non-specific adhesion of platelets. To quantify the net force acting on cells near the surface, we measured the force-separation relationships and found repulsive zones with thicknesses of 2–4 nm near the dendron surfaces. High speed (5 ms per pixel) nanoscopic force mapping further demonstrated the presence of nanoscopic defects in the dendron OEG8 monolayers. This finding suggests a lower grafting density than for OEG4, which could explain the difference in film elasticity, thickness of the repulsive zone, and cell repellency between the two dendrons. The combination of different physical techniques over different length scales helped us gain physical insights into how nanometer-thick dendron monolayers modulate the interfacial interactions between cells and oxide surfaces.

Author contributions

D. F.-F. and M. T. designed the research. D. V .N. and D. F.-F. synthesized the dendronized molecules, and J. C., W. A., C. H., E. M., O. V. K., T. H., S. K., and M. T. performed the experiments and analyzed the data. J. C., W. A., T. H., and M. T. wrote the manuscript. All authors participated in discussion and manuscript editing.

Conflicts of interest

The authors declare that there are no conflicts of interest.

Acknowledgements

D. F.-F. and M. T. thank the support from the INTERREG V Upper Rhine Program (NANOTRANSMED). T. H. and M. T. thank JSPS (KAKENHI grant numbers JP20H05210 to T. H., JP19H05719 to M. T.) for support. T. H. is thankful to Heidelberg Alumni Network, and M. T. to the German Science Foundation (SPP2171) and Nakatani Foundation for support. J. C. thanks R. Chang for experimental assistance, and M. T. thanks R. Dahint for helpful comments. We thank S. Dodds from Edanz Group (https://en-author-services.edanz.com/ac) for editing a draft of this manuscript.

Notes and references

1 Q. A. Pankhurst, J. Connolly, S. K. Jones and J. Dobson, *J. Phys. D: Appl. Phys.*, 2003, **36**, R167–R181.
2 A.-H. Lu, E. L. Salabas and F. Schüth, *Angew. Chem., Int. Ed.*, 2007, **46**, 1222–1244.
3 Y.-W. Jun, J.-H. Lee and J. Cheon, *Angew. Chem., Int. Ed.*, 2008, **47**, 5122–5135.
4 A. Jordan, R. Scholz, P. Wust, H. Schirra, S. Thomas, H. Schmidt and R. Felix, *J. Magn. Magn. Mater.*, 1999, **194**, 185–196.
5 A. Ito, M. Shinkai, H. Honda and T. Kobayashi, *J. Biosci. Bioeng.*, 2005, **100**, 1–11.
6 H. Xu, F. Yan, E. E. Monson and R. Kopelman, *J. Biomed. Mater. Res., Part A*, 2003, **66**, 870–879.
7 L. M. Lacava, Z. G. M. Lacava, M. F. Da Silva, O. Silva, S. B. Chaves, R. B. Azevedo, F. Pelegrini, C. Gansau, N. Buske, D. Sabolovic and P. C. Morais, *Biophys. J.*, 2001, **80**, 2483–2486.
8 A. K. Gupta and M. Gupta, *Biomaterials*, 2005, **26**, 3995–4021.
9 T. J. Daou, G. Pourroy, J. M. Greneche, A. Bertin, D. Felder-Flesch and S. Begin-Colin, *Dalton Trans.*, 2009, 4442–4449.
10 B. Basly, D. Felder-Flesch, P. Perriat, C. Billotey, J. Taleb, G. Pourroy and S. Begin-Colin, *Chem. Commun.*, 2010, **46**, 985–987.
11 D.-V. Nguyen, L. Hugoni, M. Filippi, F. Perton, D. Shi, E. Voirin, L. Power, G. Cotin, M.-P. Krafft, A. Scherberich, P. Lavalle, S. Begin-Colin and D. Felder-Flesch, *New J. Chem.*, 2020, **44**, 3206–3214.
12 R. Duncan and L. Izzo, *Adv. Drug Delivery Rev.*, 2005, **57**, 2215–2237.
13 T. J. Daou, S. Buathong, D. Ung, B. Donnio, G. Pourroy, D. Guillon and S. Bégin, *Sens. Actuators, B*, 2007, **126**, 159–162.
14 C. Boyer, V. Bulmus, P. Priyanto, W. Y. Teoh, R. Amal and T. P. Davis, *J. Mater. Chem.*, 2009, **19**, 111–123.
15 T. J. Daou, J. M. Grenèche, G. Pourroy, S. Buathong, A. Derory, C. Ulhaq-Bouillet, B. Donnio, D. Guillon and S. Begin-Colin, *Chem. Mater.*, 2008, **20**, 5869–5875.
16 E. L. Hanson, J. Schwartz, B. Nickel, N. Koch and M. F. Danisman, *J. Am. Chem. Soc.*, 2003, **125**, 16074–16080.
17 T. Schubert, P. C. Seitz, E. Schneck, M. Nakamura, M. Shibakami, S. S. Funari, O. Konovalov and M. Tanaka, *J. Phys. Chem. B*, 2008, **112**, 10041–10044.
18 F. F. Rossetti, E. Schneck, G. Fragneto, O. V. Konovalov and M. Tanaka, *Langmuir*, 2015, **31**, 4473–4480.
19 S. Fisk and B. Widom, *J. Chem. Phys.*, 1969, **50**, 3219–3227.
20 E. S. Wu and W. W. Webb, *J. Chem. Phys.*, 1973, **8**, 2065–2076.
21 K. Binder, *J. Chem. Phys.*, 1983, **79**, 6387–6409.
22 F. Abelès, *J. Phys. Radium*, 1950, **11**, 307–309.
23 L. G. Parratt, *Phys. Rev.*, 1954, **95**, 359–369.
24 H.-J. Butt, B. Cappella and M. Kappl, *Surf. Sci. Rep.*, 2005, **59**, 1–152.
25 J. Domke and M. Radmacher, *Langmuir*, 1998, **14**, 3320–3325.
26 S. Suresh, *Science*, 2001, **292**, 2447–2451.
27 M. F. Doerner and W. D. Nix, *J. Mater. Res.*, 1986, **1**, 601–609.
28 H. Shulha, X. Zhai and V. V. Tsukruk, *Macromolecules*, 2003, **36**, 2825–2831.
29 R. D. Frank, H. Dresbach, H. Thelen and H. G. Sieberth, *J. Biomed. Mater. Res.*, 2000, **52**, 374–381.
30 S. N. Rodrigues, I. C. Gonçalves, M. C. L. Martins, M. A. Barbosa and B. D. Ratner, *Biomaterials*, 2006, **27**, 5357–5367.
31 T. Hayashi, Y. Tanaka, Y. Koide, M. Tanaka and M. Hara, *Phys. Chem. Chem. Phys.*, 2012, **14**, 10196–10206.
32 N. Inada, H. Asakawa, Y. Matsumoto and T. Fukuma, *Nanotechnology*, 2014, **25**, 305602.
33 E. A. Mondarte, T. Maekawa, T. Nyu, H. Tahara, G. Lkhamsuren and T. Hayashi, *RSC Adv.*, 2019, **9**, 22705–22712.
34 H. P. Duwe and E. Sackmann, *Phys. A*, 1990, **163**, 410–428.
35 A. Verdaguer, G. M. Sacha, H. Bluhm and M. Salmeron, *Chem. Rev.*, 2006, **106**, 1478–1510.
36 T. A. Pascal, W. A. Goddard and Y. Jung, *Proc. Natl. Acad. Sci.*, 2011, **108**, 11794–11798.
37 W. Abuillan, A. S. Becker, B. Demé, T. Homma, H. Isobe, K. Harano, E. Nakamura and M. Tanaka, *J. Am. Chem. Soc.*, 2018, **140**, 11261–11266.
38 T. Uchihashi, M. Higgins, Y. Nakayama, J. E. Sader and S. P. Jarvis, *Nanotechnol*, 2005, **16**, S49–S53.
39 Y. Araki, T. Sekine, R. Chang, T. Hayashi and H. Onishi, *RSC Adv.*, 2018, **8**, 24660–24664.
40 L. Névot and P. Croce, *Rev. Phys. Appl.*, 1980, **15**, 761–779.
41 J. L. Hutter and J. Bechhoefer, *Rev. Sci. Instrum.*, 1993, **64**, 1868–1873.